AIP Journal of Applied Physics

A comparison of the optical properties of InGaN/GaN multiple quantum well structures grown with and without Si-doped InGaN prelayers

M. J. Davies, S. Hammersley, F. C.-P. Massabuau, P. Dawson, R. A. Oliver, M. J. Kappers, and C. J. Humphreys

Citation: Journal of Applied Physics **119**, 055708 (2016); doi: 10.1063/1.4941321

View online: http://dx.doi.org/10.1063/1.4941321

View Table of Contents: http://scitation.aip.org/content/aip/journal/jap/119/5?ver=pdfcov

Published by the AIP Publishing

A comparison of the optical properties of InGaN/GaN multiple quantum well structures grown with and without Si-doped InGaN prelayers

M. J. Davies,[1,a)] S. Hammersley,[1] F. C.-P. Massabuau,[2] P. Dawson,[1] R. A. Oliver,[2] M. J. Kappers,[2] and C. J. Humphreys[2]
[1]*School of Physics and Astronomy, Photon Science Institute, University of Manchester, Manchester M13 9PL, United Kingdom*
[2]*Department of Material Science and Metallurgy, 27 Charles Babbage Road, University of Cambridge, Cambridge CB3 0FS, United Kingdom*

(Received 27 July 2015; accepted 22 January 2016; published online 5 February 2016)

In this paper, we report on a detailed spectroscopic study of the optical properties of InGaN/GaN multiple quantum well structures, both with and without a Si-doped InGaN prelayer. In photoluminescence and photoluminescence excitation spectroscopy, a 2nd emission band, occurring at a higher energy, was identified in the spectrum of the multiple quantum well structure containing the InGaN prelayer, originating from the first quantum well in the stack. Band structure calculations revealed that a reduction in the resultant electric field occurred in the quantum well immediately adjacent to the InGaN prelayer, therefore leading to a reduction in the strength of the quantum confined Stark effect in this quantum well. The partial suppression of the quantum confined Stark effect in this quantum well led to a modified (higher) emission energy and increased radiative recombination rate. Therefore, we ascribed the origin of the high energy emission band to recombination from the 1st quantum well in the structure. Study of the temperature dependent recombination dynamics of both samples showed that the decay time measured across the spectrum was strongly influenced by the 1st quantum well in the stack (in the sample containing the prelayer) leading to a shorter average room temperature lifetime in this sample. The room temperature internal quantum efficiency of the prelayer containing sample was found to be higher than the reference sample (36% compared to 25%) which was thus attributed to the faster radiative recombination rate of the 1st quantum well providing a recombination pathway that is more competitive with non-radiative recombination processes.
[http://dx.doi.org/10.1063/1.4941321]

I. INTRODUCTION

InGaN/GaN multiple quantum well (MQW) active regions grown on *c*-plane substrates are widely used in efficient light emitting diodes (LEDs).[1–3] The high recombination efficiencies of these InGaN/GaN QWs occur despite high densities of extended crystal defects[4–6] and the large built-in electric fields perpendicular to the plane of the QWs.[7–9] These electric fields result in a spatial separation of the electron and hole wavefunctions, leading to a reduction in the radiative recombination rate and an associated Quantum Confined Stark Effect (QCSE). As the internal quantum efficiency (IQE) is determined by competition between radiative and non-radiative recombination processes, slower radiative recombination rates can limit the IQE. It has been reported[10–19] that the inclusion of an InGaN layer prior to the deposition of the 1st QW, a so-called "prelayer," can lead to significant improvements in the IQE of InGaN multiple QW structures and LEDs. Typical prelayer structures consist of 20–30 nm of intentionally Si-doped (In)GaN, which can be either a single layer or a short-period superlattice, positioned a few nanometers beneath the 1st QW. The improvements in IQE have been attributed to either increases in the radiative recombination rate[15,16,18,20,21] or decreases in the non-radiative recombination rate.[11,19] Nanhui *et al.*[15,16] reported that the inclusion of an unintentionally doped 20 nm thick $In_{0.08}Ga_{0.92}N$ layer in an InGaN/GaN multiple QW structure led to an increase in the photoluminescence (PL) intensity at room temperature. This was attributed to strain relaxation in the QWs which led to a reduction in the strength of the built-in electric field and hence increasing the radiative recombination rate. However, it should be noted that no direct experimental evidence for strain relaxation was found. Otsuji *et al.*[10] and Takahashi *et al.*[12] reported an increase in the electroluminescence (EL) intensity of a three-period $In_{0.3}Ga_{0.7}N$/GaN multiple QW device, over a range of temperatures, when including a 15 nm thick Si-doped $In_{0.18}Ga_{0.82}N$ prelayer beneath the QW stack. The increase in intensity was ascribed, in both reports, to an enhancement of the electron capture efficiency, due to the prelayer behaving as an electron reservoir. Xia *et al.*[22] reported a similar explanation for a measured increase in cathodoluminescence (CL) intensity in a depth resolved CL investigation and thus concluded that some charge transfer occurs between the InGaN prelayer and the QWs. Akasaka *et al.*[13,14] and Törmä *et al.*[11] both reported that prelayers led to increases in the PL and EL

a)Matthew.Davies-2@Manchester.ac.uk

intensities at room temperature; this behaviour was ascribed to a reduction in the density of defects in the vicinity of the QWs. Takahashi *et al.*[23] reported that the inclusion of low temperature grown GaN and InGaN prelayers beneath InGaN/GaN single QWs resulted in an increased formation probability of "V"-defects, which are believed to create potential barriers around threading dislocations, thereby inhibiting carrier capture by these extended defects.[24] However, this is somewhat contradictory to the results of the investigation of Nanhui *et al.*,[15,16] in which the authors report a reduction in "V"-defect density associated with the inclusion of a prelayer. We have presented initial results[17] on the effect of including an InGaN:Si prelayer before a MQW stack. We reported a greater room temperature PL IQE for an MQW structure grown with a prelayer compared with one grown without. Also along with the improvement in IQE, we noted the presence of a feature in the PL spectrum 70 meV above the main PL peak. The improvement in the room temperature IQE was tentatively ascribed to this additional recombination process. The high energy emission was attributed to either carrier recombination in QWs that form on the semi-polar facets of the "V" defects or to the 1st QW in the MQW stack whose properties had been modified by the InGaN prelayer. Subsequently, we have shown[20,21] that the inclusion of a doped GaN or InGaN prelayer beneath a single QW leads to a large blue shift of the PL peak emission energy and a significant reduction in the low temperature (10 K) PL decay time at the PL peak, compared to a single QW structure grown without a prelayer. These observations are compatible with the results of calculations performed using nextnano[3] (nextnano GmbH) which showed a significant reduction in the electric field across the single QW for each structure containing a prelayer due to an enhancement of the surface polarisation field, which opposed the built-in electric field across the QW.[9,20,21] The reduction in electric field across the QW results in an increase in the electron-hole wavefunction overlap, thus leading to an increase in the radiative recombination rate, and a reduction in the QCSE. In light of this recent work, we have extended our investigations of InGaN MQWs with prelayers to include further PL excitation (PLE) spectroscopy and a detailed temperature dependent time-resolved spectroscopic study of the optical properties of InGaN MQWs with and without prelayers.

II. EXPERIMENTAL DETAILS

Two MQW structures, with and without an InGaN prelayer, were grown by metalorganic vapour phase epitaxy on *c*-plane sapphire substrates in a Thomas Swan close-coupled showerhead reactor. The structures were grown using the "quasi-two temperature" growth method[25] and the QWs consisted of 10 periods of $In_xGa_{1-x}N$ QWs, separated by GaN barriers. X-ray diffraction measurements (XRD), using the method of Vickers *et al.*,[26] showed that the indium fraction of the QWs in both the samples A and B was $0.16(\pm 0.01)$, with QW thicknesses of $2.5(\pm 0.1)$ nm and barrier thicknesses of $7.5(\pm 0.1)$ nm. Sample A did not contain a prelayer, whereas sample B contained a 24 nm thick Si-doped (5×10^{18} cm^{-3}) $In_{0.05}Ga_{0.95}N$ prelayer grown at 770 °C separated from the 1st QW in the stack by 3 nm of unintentionally doped GaN (the thickness and composition of the prelayer were also determined by XRD). Complementary to the XRD measurements, which showed the average indium fraction of all the QWs in the structures, high resolution transmission electron microscopy was used to conduct a geometric phase analysis[27] of each individual QW in sample B. No variation in the indium composition of the individual QWs (within ± 0.01) or QW thickness (within ± 0.2 nm) could be observed. Furthermore, in our previous studies of single QW structures deposited on various prelayers,[20,21] we observed no apparent modification of the indium composition or thickness of the QW as a consequence of including the prelayers. In a previous report[17] of the properties of these MQW structures with and without a prelayer no evidence of strain relaxation of the QWs was found; thus we were able to rule out strain relaxation as a possible mechanism for any change in the optical properties of these structures.

The optical properties of the structures were studied using a combination of PLE spectroscopy, temperature dependent (time-integrated) PL spectroscopy and PL decay time measurements. Temperature dependent measurements were performed by mounting the samples on the cold finger of a temperature controlled closed-cycle helium cryostat. For all the PL measurements, the samples were mounted at Brewster's angle with respect to the PL collection axis in order to minimise the effects of Fabry-Pérot interference on the PL spectra. For all the spectra presented in Fig. 1 the efficiency of the PL collection was not the same, so the indicated intensities of the PL spectra are not comparable between samples. A frequency tripled mode-locked Ti:sapphire laser emitting photons of 4.881 eV and a 300 W xenon lamp coupled

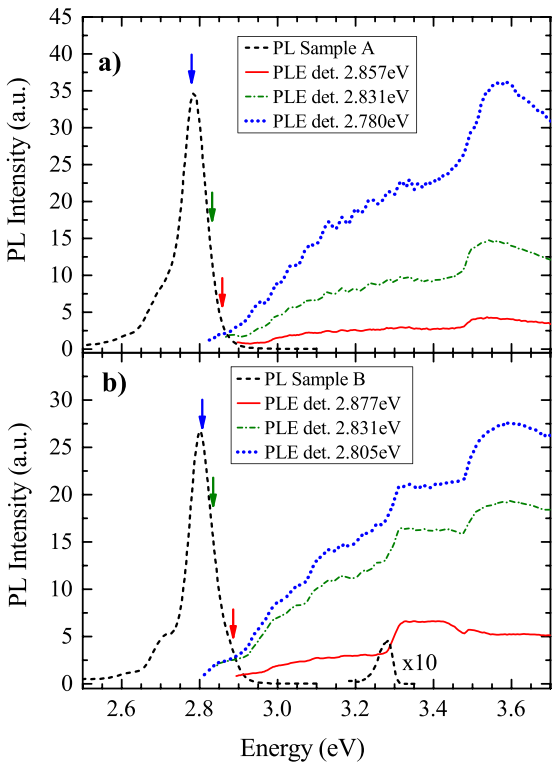

FIG. 1. Low temperature (10 K) PL spectra and PLE spectra detected at the detection energies indicated in the figure for (a) sample A and (b) sample B.[17]

with a 0.25 m monochromator were used as excitation sources for the PL spectroscopy. The time-averaged excitation power density of the pulsed laser was $6\,W\,cm^{-2}$ (100 fs pulses with repetition rate of 800 kHz), with an excitation spot area of $2 \times 10^{-5}\,cm^2$. The excitation power density of the lamp source was approximately $100\,\mu W\,cm^{-2}$, with an excitation area of $0.02\,cm^2$. The lamp/monochromator combination was also used as a continuously tuneable excitation source for the PLE measurements. The PL decay time measurements were performed using excitation by the Ti:sapphire laser with the signal processed by a time-correlated single photon counting system.

III. RESULTS AND DISCUSSION

The low temperature (10 K) PL spectra for samples A (reference) and B (with prelayer), excited using the Xe lamp/monochromator combination with photon energy 3.647 eV, are shown in Figs. 1(a) and 1(b), respectively. The energy of the main PL peak is 2.784 eV for sample A and 2.801 eV for sample B. The main PL peak in such spectra is attributed to recombination of localised electrons and holes in the QWs.[28,29] The low energy emission features occurring at multiples of ~90 meV below the main emission peaks are attributed to longitudinal optical (LO) phonon replicas of the main QW emission peaks.[30] The additional small feature at 3.27 eV in the spectrum from sample B is attributed to recombination in the InGaN prelayer.[17]

The PLE spectra recorded at 10 K for various detection energies across the PL spectra of both samples are also shown in Figs. 1(a) and 1(b). The PLE spectrum from sample A detected at 2.780 eV shows relatively strong PL intensity for photon energies greater than 3.5 eV. Above 3.5 eV carriers are excited in the GaN close to the QWs and they are then captured mainly by the QWs. When the excitation photon energy drops below 3.5 eV the only significant carrier excitation occurs in the optically thin InGaN QWs which leads to a reduction in the excited carrier density and a subsequent drop in PL intensity. The absorption spectrum of InGaN/GaN QWs is subject to significant inhomogeneous broadening, which is attributed to a combination of the QCSE, the quantum confined Franz-Keldysh effect,[31–33] and the effects of alloy disorder,[29,34] and thus as the excitation photon energy is reduced further (below 3.3 eV), the PL intensity falls off progressively rather than exhibiting a sharp cut off at the sub band edge as might be expected. The oscillations observed on the PLE spectra at photon energies below 3.5 eV occur as a consequence of multiple beam interference effects in the sample. The general form of the PLE spectra from sample A does not change when the detection energy is varied from 2.780 to 2.857 eV, as shown in Fig. 1(a).

The PLE spectrum detected at 2.805 eV for sample B (near the peak of the 10 K PL spectrum) shows the same features as the PLE spectra in Fig. 1(a) as well as a new feature for excitation photon energies between 3.3 and 3.5 eV. Absorption measurements reported by McCluskey *et al.*[35] determined the room temperature bandgap of a strained $In_{0.054}Ga_{0.946}N$ epilayer to be 3.251 eV. Thus by applying the correction for the temperature dependence of the bandgap,[36] we calculate the bandgap energy for an $In_{0.054}Ga_{0.946}N$ strained layer to be 3.31 eV. This estimate of the 10 K bandgap is very close to the low energy side of our measured absorption edge, and therefore we assign this feature to the excitation of carriers in the $In_{0.05}Ga_{0.95}N$ prelayer. In order to verify this assignment, we need to understand how and why excitation of carriers in the prelayer can lead to an increase in the intensity of the QW emission at a temperature of 10 K. Further information is revealed when we consider the strength of the prelayer excitation feature as a function of detection energy as shown in Fig. 1(b). As the detection energy is increased, the prelayer feature becomes progressively stronger compared with that associated with direct excitation of carriers in the QWs. This suggests that there is a separate recombination path on the high energy side of the PL spectrum that is particularly sensitive to excitation of carriers in the prelayer, and indeed close inspection of the high energy side of the PL spectrum reveals a distinct shoulder around 2.87 eV which we will refer to as the *X*-band. The relative strength of the *X*-band is, as can be anticipated from the PLE spectra, strongly dependent on the excitation energy. In Fig. 2 are shown three PL spectra excited with different photon energies. The excitation photon energy of 3.647 eV results, to varying degrees, in excitation of carriers in the GaN layers, the prelayer, and the QWs, while a photon energy of 3.397 eV excites carriers in the prelayer and the QWs, and 3.139 eV results in excitation of carriers in the QWs only. A multiple Gaussian fitting approach was used to model the main emission at 2.802 eV and the emission from the *X*-band, under each of the excitation regimes. The multiple Gaussian fitting functions contained up to two LO phonon replicas of the emission peaks.

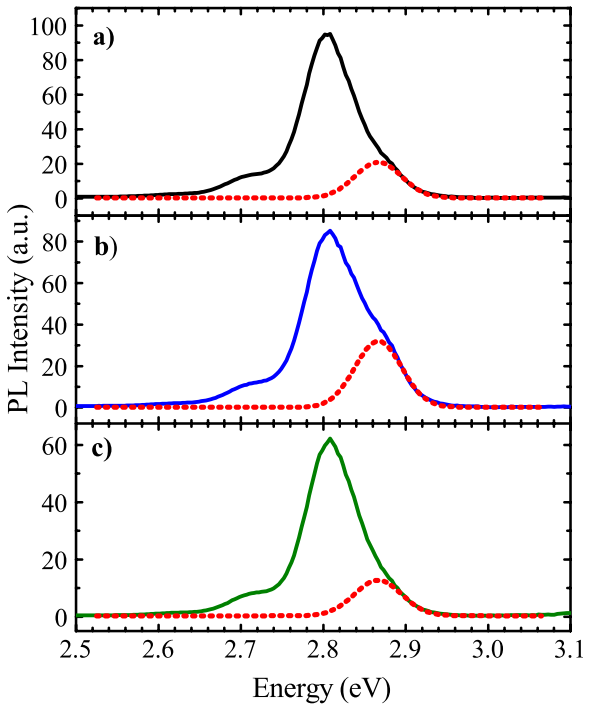

FIG. 2. Low temperature (10 K) PL spectra measured using different excitation photon energies, (a) 3.647 eV, (b) 3.397 eV, and (c) 3.139 eV, along with the Gaussian fits of the *X*-band emission in each spectrum (dashed lines).

The Gaussian fit of the *X*-band emission in each excitation regime is also shown in Fig. 2 and indicates that the *X*-band is centred at approximately 2.865(±0.005) eV with a similar full width at half maximum to the 2.802 eV emission peak. The *X*-band can be easily seen in the PL spectrum excited with 3.397 eV energy photons (carrier excitation in prelayer and QWs) as the strength of the *X*-band is stronger than in the other two cases.

To determine the overall effects of the prelayer on the QWs and, in particular, the origin of the *X*-band, the conduction and valence band profiles of both structures were calculated using the commercially available package nextnano[3]. The conduction and valence band edge profiles are strongly influenced by the position of the Fermi energy in different regions of the structure. Mayrock *et al.*[9] reported that the high density of unpaired bonds at the surface of Ga-terminated GaN epilayers results in a large surface charge, sufficient to pin the Fermi level at the valence band edge. Mayrock *et al.*[9] subsequently showed that in *n*-type GaN epilayers, this pinning of the Fermi level at the surface results in a significant bending of the conduction and valence bands and a surface polarisation field acting in the growth direction (+*c*). The presence and subsequent modification of this surface polarisation field has been reported to significantly influence the properties of InGaN/GaN QWs.[20,21,37–39] We have reported[20,21] that this surface polarisation field is significantly modified by the inclusion of Si-doped prelayers, leading to a reduction in the total electric field across the QW in single QW structures.

The calculated conduction and lowest energy valence band edge profiles for samples A and B are shown in Fig. 3, where the Fermi energy is 0 eV. The electric field across an InGaN/GaN QW is determined by the combined effects of the discontinuities in spontaneous polarisation and piezoelectric polarisation at the interfaces of the InGaN layer and the surface polarisation field. In sample A, an electric field of 240 mV nm^{-1} (−*c*) is calculated for each QW, as shown in the inset of Fig. 3(a). The inclusion of the Si-doped (5×10^{18} cm^{-3}) InGaN prelayer in sample B and the subsequent pinning of the Fermi level near the conduction band edge at a distance 105 nm from the surface result in an increase of the surface polarisation field so that the electric field across the majority of the QWs in sample B is reduced to 212 mV nm^{-1}, as shown in the inset of Fig. 3(b). In addition, the electric field in QW #1, the QW closest to the prelayer, is further reduced to 186 mV nm^{-1}. The cause of this additional reduction in electric field was identified previously[21] as being due to the interaction between charges at the QW interfaces and the upper charged interface of the prelayer. Thus, we predict that the effect of the prelayer is, in comparison with the sample without a prelayer, to reduce the electric fields by similar amounts across QWs #2–10 with a much greater reduction in the field across QW #1. Therefore, we would anticipate a reduction in the QCSE for QWs #2–10 with a much greater reduction for QW #1. This suggests that the peak recombination energy of sample B would occur at a greater energy than sample A, as we observe. Furthermore, we also predict a distinct recombination feature associated with QW #1 at a higher energy than the other QWs in sample B. Therefore, we assign the *X*-band

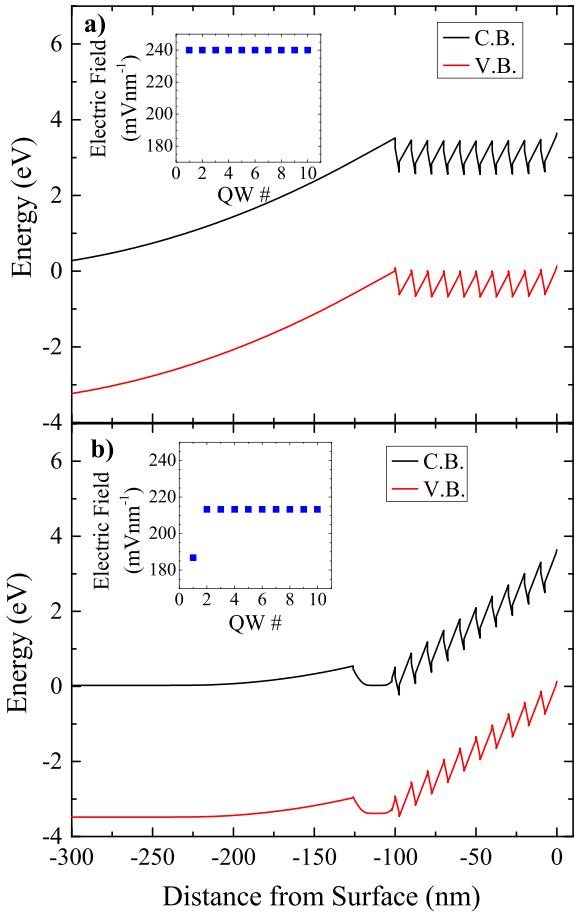

FIG. 3. Calculated conduction (CB) and valence band (VB) edge energies for (a) sample A and (b) sample B, where the Fermi energy is 0 eV. Insets show the calculated electric field across each QW.

as being due to carrier recombination in the 1st QW. Based on the preceding assignment for the *X*-band, we are now in a position to discuss some of the details of the PLE spectra from sample B. In the discussion above, we suggested that the feature between 3.3 and 3.5 eV was due to excitation of carriers in the InGaN prelayer. For this process to be reflected in the PLE spectra, it demands that the carriers created in the prelayer are able to transfer to the emitting state being monitored, implying in this case transfer into the 1st QW in the stack. Based on the band profile in Fig. 3(b), we propose that the photo-excited holes relax into QW #1. As for the electrons (ignoring any Coulomb interaction between the photo-excited electrons and holes), we suggest that electrons are able to tunnel from the prelayer through the thin barrier layer between the prelayer and QW #1. This overall view of the carrier excitation and transfer processes into QW #1 can be used to explain more of the details of the PLE spectrum of sample B. In particular, as seen in Fig. 1(b), when detecting emission (2.87 eV) primarily from the *X*-band at photon energies greater than the GaN bandgap, the PL intensity is lower than when excited with light with energy between 3.3 and 3.5 eV. This behaviour is opposite to that in the PLE spectra obtained when monitoring the emission intensity at the peak of the emission spectrum of sample B (2.805 eV) and all the PLE spectra from sample A. The higher intensity of the *X*-band when excited with photon

energy between 3.3 and 3.5 eV occurs as a consequence of the strong absorption of light of energy >3.5 eV in the QWs and barriers above QW #1, and thus before it reaches the region of QW #1 and prelayer. However, the light of energy <3.5 eV is only weakly absorbed and capable of exciting a significant carrier density in the prelayer, of which a significant fraction transfers to QW #1. So overall, the prelayer excitation feature appears more strongly in the PLE spectrum when detected on the *X*-band because the carriers that are excited in the GaN layers closer to the surface of the structure are prevented from being captured by QW #1 due to the preferential capture by the QWs which are closer to the region of excitation. We regard this behaviour as further evidence that the *X*-band involves emission from QW #1 at the bottom of the QW stack.

To understand how the prelayer influences the room temperature IQE,[17] we turn our attention to the temperature dependence of the optical properties. Time-integrated PL spectra and PL decay transients were recorded for both samples at temperatures between 10 and 300 K, using light with a photon energy of 4.881 eV so that carriers were excited into the GaN barriers as well as into the QWs (in both samples) and also the prelayer in sample B. In general, the low temperature (10 K) PL decay transients measured from InGaN/GaN QWs are non-exponential.[20,28,40–42] This non-exponential nature is attributed to variations in the in-plane overlap of the electron and hole wavefunctions[28] and so a single time constant cannot be used to define the entire decay curves. Examples of the decays curves from samples A and B are shown in Fig. 4. We therefore use the time (τ_e) required for the PL intensity to decay by a factor of $1/e$ from the maximum intensity to characterise each decay transient. The low temperature PL decay times of InGaN/GaN QWs are also reported[28,30,41–44] to vary at different detection energies across the zero phonon line, with an increase in decay time as the detection energy is reduced. This effect has been explained as follows: as the detection energy is reduced, we detect carriers that are localised in regions of progressively increasing In fraction where the local built-in electric field is stronger, thus leading to a reduction in electron-hole wavefunction overlap.[30,41,44] Time-integrated PL spectra and extracted PL decay times, τ_e, measured at different energies across the spectra as a function of temperature are shown in Fig. 5 for sample A and Fig. 6 for sample B. A range of time-averaged power densities, between 120 mW cm^{-2} and 12.5 W cm^{-2} with 100 fs pulses and 800 kHz repetition rate, were investigated; in this excitation power density range, no evidence of carrier field screening was observed. The excitation conditions presented in Figs. 5 and 6 were a time-averaged power density of 6 W cm^{-2}.

To understand the role of the prelayer and *X*-band in the recombination dynamics, we must first understand the temperature dependent behaviour exhibited by sample A. As discussed above, a strong reduction in PL decay time occurs at 10 K towards the high energy side of the spectrum, with a measured decay time of 16(±2) ns detected at 2.744 eV to 10(±1) ns at 2.802 eV (PL peak) to 2(±0.2) ns detected at 2.897 eV, reflecting the inherent variation in radiative recombination rate amongst the localised states.[28,30,41,44] The difference in PL peak energy at 10 K, in each sample, when measured using the lamp or laser sources occurs because the region excited by the two sources contains QWs with different In contents. This is due to the variation in In fraction in the QWs across the wafers as described earlier. When the temperature was increased to 100 K, the overall characteristics of the spectral dependence of the decay curves remain essentially unchanged apart from, as reported by Badcock *et al.*,[41] changes in the carrier dynamics due to carrier

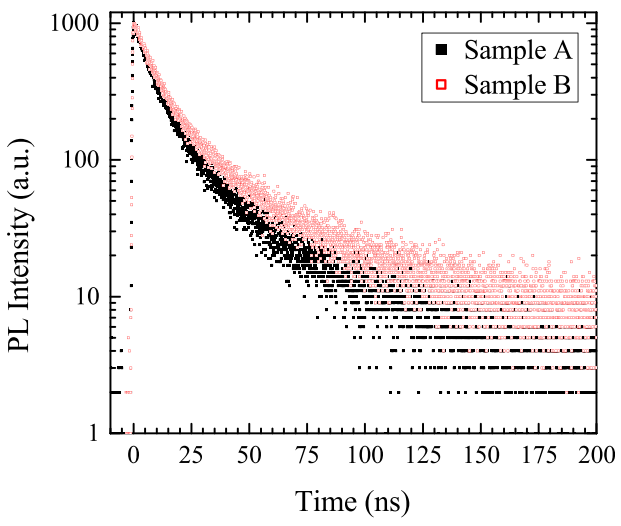

FIG. 4. Low temperature (10 K) PL decay transients detected at the peaks of the PL spectra of samples A and B.

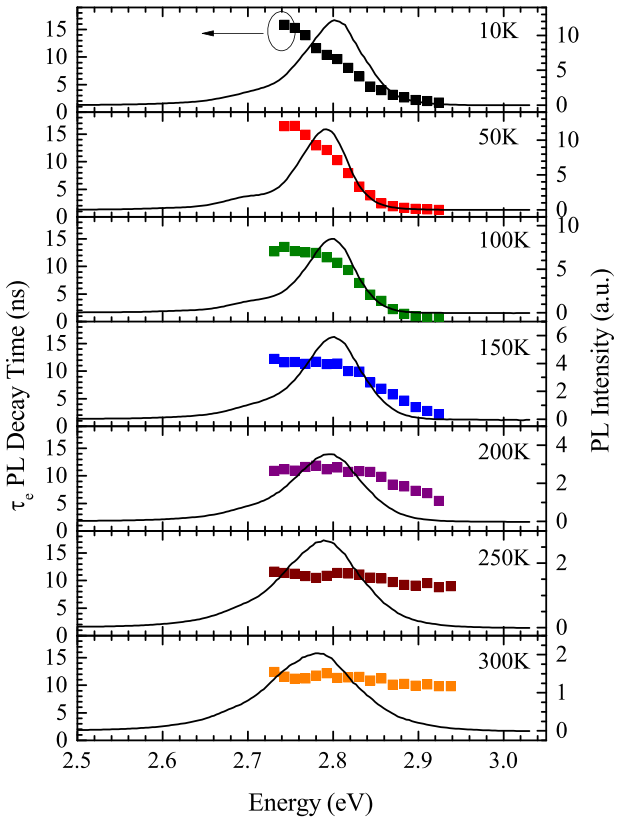

FIG. 5. τ_e values for sample A measured at various detection energies across the spectrum, along with the time integrated PL spectra, excited with the pulsed laser, for temperatures between 10 and 300 K.

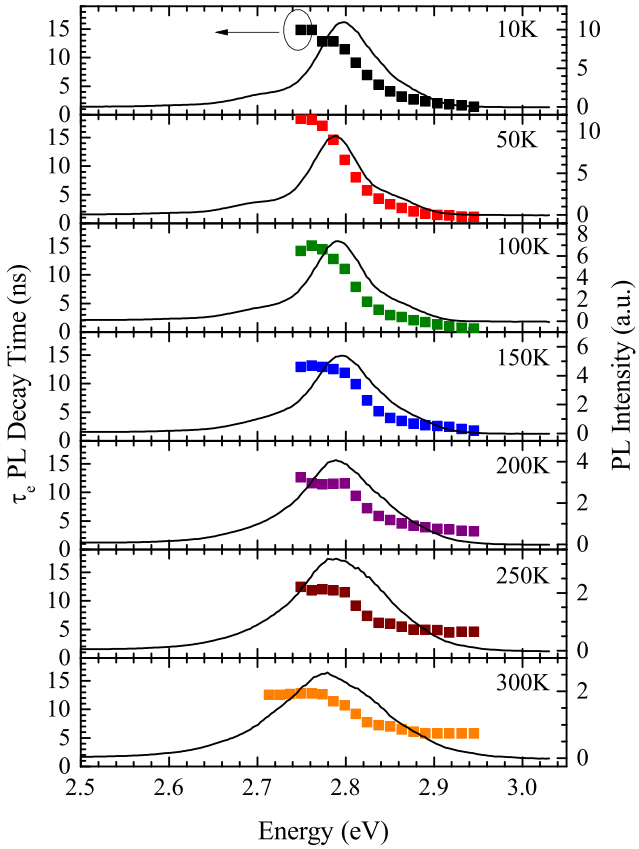

FIG. 6. τ_e values for sample B measured at various detection energies across the spectrum, along with the time integrated PL spectra, excited with the pulsed laser, for temperatures between 10 and 300 K.

hopping reflected in the low temperature regime of the "S"-shape temperature dependence[29,45–49] of the peak emission energy as a function of temperature. On increasing the temperature further from 100 to 300 K, as can be seen in Fig. 5, the PL spectra broaden due to thermalisation of carriers across the range of localised states.[29,45–47,50–52] Over this temperature range, the decay times at the PL peak and on the low energy side of the spectra remain constant $\sim$11($\pm$1) ns, while the decay times on the high energy side of the spectra increase progressively with increasing temperature, such that at 300 K the decay time is essentially constant across the spectrum. This suppression of the spectral dependence of the PL decay time with increasing temperature has been reported by several groups.[49,53–56] In these works,[49,53–55] the measured decay curves at room temperature were single exponential and independent of detection energy which was ascribed to the effects of non-radiative recombination. However, the samples discussed here are quite efficient at 300 K with IQEs of 25($\pm$2)% and 36($\pm$2)% for sample A and sample B, respectively. The room temperature PL IQE was determined by comparing the integrated PL intensity at 10 K with that at 300 K, using the assumption that the recombination at 10 K is purely radiative and hence is 100% efficient. Therefore, we might expect the room temperature decay curves to be made up of radiative and non-radiative components. The usual methodology to extract the time constants for the different processes is to use the measured time constant with the absolute IQE values. This is not possible in our case as the decays, even at 300 K, are non-exponential and thus we cannot assign a unique time constant to the data. Yet the overall time scale of the recombination coupled with the non-exponential character of the decays suggests that the decay curves are strongly influenced by the radiative processes. Therefore, we ascribe the constant decay time measured across the spectrum at 300 K as being a consequence of the carrier redistribution process responsible for the high temperature component of the "S"-shape temperature dependence of the peak energy. In light of the relatively large value of the IQE for sample A and the non-exponential form of the decay curves which occur on a very similar time scale to those at low temperature, we believe that the decay kinetics are strongly influenced by the non-exponential radiative decay component which is indicative of localised carrier emission. The most significant difference between the recombination dynamics measured at 10 K and at 300 K is that at 10 K a strong spectral dependence of the form of the decay curves is observed, whereas at 300 K the form of the decay curves is independent of detection energy. This we believe is in line with the work of Wang *et al.*[57] who reported that at sufficiently high temperatures, localised carriers in InGaN QWs can come into a thermalised distribution on a time scale of the order of hundreds of ps. As the time for these processes is much shorter than the characteristic time decays in sample A, we assign the energy independent decay curves as being due to recombination of a thermalised localised carrier population. This thermalised carrier population argument is in line with the explanation for the anomalous peak shift as a function of temperature around 300 K. So the common decay lifetime measured at all detection energies will reflect some average of the radiative recombination lifetimes of all the localised states, caused by the local variations in the In concentration, in the nominally identical QWs.

Turning our attention now to sample B which contains the prelayer, the results of the temperature and spectral dependence of τ_e are shown in Fig. 6. At 10 K, the PL decay times measured across the PL spectrum again vary strongly with increasing detection energy, from 15($\pm$2) ns at 2.749 eV to 11($\pm$1) ns at 2.798 eV (PL peak) to 2($\pm$0.2) ns detected at 2.904 eV. Just as for sample A, this variation in decay time when detecting across the PL spectrum can be largely attributed to the variation in the radiative recombination rate amongst the localised states. Also there is no distinct change in the spectral dependence of the decay time when we detect the *X*-band. This is despite the predicted change in electric field in QW #1. We believe that the reasons for this are twofold. At a temperature of 10 K, the dominant main emission band and the *X*-band overlap strongly so any PL decay curve will contain some admixture of the separate decay processes. Furthermore, we would not expect the form of the decay curves from the *X*-band emission to be significantly different from that involving the weakly localised states on the high energy side of the main emission band as they both are governed by relatively small values of the electric field. As the temperature is increased to 100 K, we again see the same behaviour in the dynamics that we observed in sample A. At a temperature of 100 K, where the width of the

main emission line has decreased, we can clearly resolve the *X*-band with a peak energy ~2.86 eV. For temperatures ≥150 K, the spectral dependence of the decay time is different from that observed for sample A. In this temperature range, the decay time measured at the PL peak and on the low energy side of the main emission remains constant at 12(±1) ns, whereas the decay time measured across the *X*-band (detected in the range 2.835–2.950 eV) also remains constant at any one temperature but increases progressively from 2(±1) ns at 150 K to 6(±1) ns at 300 K. Thus at 300 K, the overall spectral dependence of the decay time is made up of two distinct regions with decay times of 6(±1) ns and 12(±1) ns. The changeover between these two regions occurs around 2.82 eV, i.e., when we move from detecting emission from the majority of the QWs to the *X*-band.

As discussed for sample A, due to the relatively high IQEs measured for these samples, the constant decay time measured across the PL spectra is attributed to an "average" decay time due to the rapid carrier redistribution processes amongst the localised states in a given QW. Therefore, the step change in decay times measured in sample B is attributed to the difference in "average" decay rate between QWs #2–10 and the *X*-band emission from QW #1, which includes a faster radiative component due to the smaller electric field across the QW. Based on the above discussion, we are now in a position to explain the differences in IQE values at 300 K. The temperature dependent PL decay time measurements reveal that modification of the QCSE in QW #1 results in emission occurring at a higher energy than the emission of QWs #2–10 (giving rise to the *X*-band) and with a faster radiative recombination rate. Thus, the overall spectrum from sample B contains a component (the *X*-band) that is more able to compete with non-radiative recombination processes, whereas, of course, sample A does not contain this modified QW. Therefore, we attribute the greater room temperature IQE in sample B to the emission from QW #1, which is a more efficient recombination channel than the rest of the spectrum.

IV. CONCLUSIONS

In summary, we have performed a comparative investigation of two multiple QW structures that were grown with and without an $In_{0.05}Ga_{0.95}N$ Si-doped prelayer. At low temperature (10 K), a distinct high energy emission band (which we have referred to as the *X*-band) at ~70 meV above the main emission peak was observed in the PL spectrum of the sample with the prelayer. Band structure calculations of both samples showed that the presence of the Si-doped prelayer results in a modification of the electric field across the entire multiple QW stack, as a consequence of a modification of the surface polarisation field of the structure.[20,21] The band structure calculations also revealed a greater reduction of the electric field in QW #1 in the structure with a prelayer to which we ascribe the origin of the *X*-band emission. The reduced electric field in QW #1 thus leads to a significant reduction in the QCSE and a faster radiative recombination rate, leading to a shorter "average" decay time at room temperature in this QW. The faster radiative recombination rate of QW #1 (the *X*-band emission) thus leads to enhanced competition with non-radiative recombination processes at elevated temperatures. We therefore ascribe the increase in room temperature IQE from 25(±2)% to 36(±2)% to the reduction in QCSE of QW #1, resulting in the higher energy *X*-band emission, such that carrier recombination in QW #1 is less susceptible to non-radiative recombination processes due to the increase in the radiative recombination rate of that QW caused by the prelayer. This modification of the carrier dynamics induced by the prelayer may have a significant impact on the design of LED structures.

ACKNOWLEDGMENTS

This work was carried out with the financial support of the United Kingdom Engineering and Physical Sciences Research Council under Grant Nos. EP/I012591/1 and EP/H011676/1.

[1]Q. Dai, M. F. Schubert, M. H. Kim, J. K. Kim, E. F. Schubert, D. D. Koleske, M. H. Crawford, S. R. Lee, A. J. Fischer, G. Thaler, and M. A. Banas, Appl. Phys. Lett. **94**, 111109 (2009).
[2]A. Hangleiter, D. Fuhrmann, M. Grewe, F. Hitzel, G. Klewer, S. Lahmann, C. Netzel, N. Riedel, and U. Rossow, Phys. Status Solidi A **201**, 2808 (2004).
[3]Y. L. Li, Y. R. Huang, and Y. H. Lai, Appl. Phys. Lett. **91**, 181113 (2007).
[4]S. Nakamura, M. Senoh, and T. Mukai, Appl. Phys. Lett. **62**, 2390 (1993).
[5]S. Nakamura, T. Mukai, and M. Senoh, Appl. Phys. Lett. **64**, 1687 (1994).
[6]M. J. Davies, P. Dawson, F. C.-P. Massabuau, F. Oehler, R. A. Oliver, M. J. Kappers, T. J. Badcock, and C. J. Humphreys, Phys. Status Solidi C **11**, 750 (2014).
[7]T. Takeuchi, S. Sota, M. Katsuragawa, M. Komori, H. Takeuchi, H. Amano, and I. Akasaki, Jpn. J. Appl. Phys., Part 2 **36**, L382 (1997).
[8]F. Bernardini, V. Fiorentini, and D. Vanderbilt, Phys. Rev. B **63**, 193201 (2001).
[9]O. Mayrock, H.-J. Wünsche, and F. Henneberger, Phys. Rev. B **62**, 16870 (2000).
[10]N. Otsuji, K. Fujiwara, and J. K. Sheu, J. Appl. Phys. **100**, 113105 (2006).
[11]P. T. Törmä, O. Svensk, M. Ali, S. Suihkonen, M. Sopanen, M. A. Odnoblyudov, and V. E. Bougrov, J. Cryst. Growth **310**, 5162 (2008).
[12]Y. Takahashi, A. Satake, K. Fujiwara, J. K. Shue, U. Jahn, H. Kostial, and H. T. Grahn, Phys. E **21**, 876 (2004).
[13]T. Akasaka, H. Gotoh, T. Saito, and T. Makimoto, Appl. Phys. Lett. **85**, 3089 (2004).
[14]T. Akasaka, H. Gotoh, Y. Kobayashi, H. Nakano, and T. Makimoto, Appl. Phys. Lett. **89**, 101110 (2006).
[15]N. Nanhui, W. Huaibing, L. Jianping, L. Naixin, X. Yanhui, H. Jun, D. Jun, and S. Guangdi, J. Cryst. Growth **286**, 209 (2006).
[16]N. Nanhui, W. Huaibing, L. Jianping, L. Naixin, X. Yanhui, H. Jun, D. Jun, and S. Guangdi, Solid-State Electron. **51**, 860 (2007).
[17]M. J. Davies, F. C.-P. Massabuau, P. Dawson, R. A. Oliver, M. J. Kappers, and C. J. Humphreys, Phys. Status Solidi C **11**, 710 (2014).
[18]T. Li, Q. Y. Wei, A. M. Fischer, J. Y. Huang, Y. U. Huang, F. A. Ponce, J. P. Liu, Z. Lochner, J.-H. Ryou, and R. D. Dupuis, Appl. Phys. Lett. **102**, 041115 (2013).
[19]A. M. Armstrong, B. N. Bryant, M. H. Crawford, D. D. Koleske, S. R. Lee, and J. J. Wierer, J. Appl. Phys. **117**, 134501 (2015).
[20]M. J. Davies, P. Dawson, F. C.-P. Massabuau, R. A. Oliver, M. J. Kappers, and C. J. Humphreys, Appl. Phys. Lett. **105**, 092106 (2014).
[21]M. J. Davies, P. Dawson, F. C.-P. Massabuau, A. L. Fol, R. A. Oliver, M. J. Kappers, and C. J. Humphreys, Phys. Status Solidi B **252**, 866 (2015).
[22]Y. Xia, W. Hou, L. Zhao, M. Zhu, T. Detchprohm, and C. Wetzel, IEEE Trans. Electron Devices **57**, 2639 (2010).
[23]H. Takahashi, A. Ito, T. Tanaka, A. Watanabe, H. Ota, and K. Chikuma, Jpn. J. Appl. Phys., Part 2 **39**, L569 (2000).
[24]A. Hangleiter, F. Hitzel, C. Netzel, D. Fuhrmann, U. Rossow, G. Ade, and P. Hinze, Phys. Rev. Lett. **95**, 127402 (2005).
[25]S. J. Leem, Y. C. Shin, E. H. Kim, C. M. Kim, B. G. Lee, Y. Moon, I. H. Lee, and T. G. Kim, Semicond. Sci. Technol. **23**, 125039 (2008).

[26]M. E. Vickers, M. J. Kappers, T. M. Smeeton, E. J. Thrush, J. S. Barnard, and C. J. Humphreys, J. Appl. Phys. **94**, 1565 (2003).
[27]M. Hýtch, E. Snoeck, and R. Kilaas, Ultramicroscopy **74**, 131 (1998).
[28]A. Morel, P. Lefebvre, S. Kalliakos, T. Taliercio, T. Bretagnon, and B. Gil, Phys. Rev. B **68**, 045331 (2003).
[29]P. G. Eliseev, M. Osinski, J. Lee, T. Sugahara, and S. Sakai, J. Electron. Mater. **29**, 332 (2000).
[30]D. M. Graham, A. Soltani-Vala, P. Dawson, M. J. Godfrey, T. M. Smeeton, J. S. Barnard, M. J. Kappers, C. J. Humphreys, and E. J. Thrush, J. Appl. Phys. **97**, 103508 (2005).
[31]S. Chichibu, T. Azuhata, T. Sota, and S. Nakamura, Appl. Phys. Lett. **69**, 4188 (1996).
[32]S. F. Chichibu, A. C. Abare, M. S. Minsky, S. Keller, S. B. Fleischer, J. E. Bowers, E. Hu, U. K. Mishra, L. A. Coldren, S. P. DenBaars, and T. Sota, Appl. Phys. Lett. **73**, 2006 (1998).
[33]C. Sasaki, M. Iwata, Y. Yamada, T. Taguchi, S. Watanabe, M. Minsky, T. Takeuchi, and N. Yamada, Phys. Status Solidi B **228**, 133 (2001).
[34]W. Shan, W. Walukiewicz, E. E. Haller, B. D. Little, J. J. Song, M. D. McCluskey, N. M. Johnson, Z. C. Feng, M. Schurman, and R. A. Stall, J. Appl. Phys. **84**, 4452 (1998).
[35]M. D. McCluskey, C. G. Van de Walle, L. T. Romano, B. S. Krusor, and N. M. Johnson, J. Appl. Phys. **93**, 4340 (2003).
[36]Q. Guo and A. Yoshida, Jpn. J. Appl. Phys., Part 1 **33**, 2453 (1994).
[37]L. H. Peng, C. W. Shih, C. M. Lai, C. C. Chuo, and J. I. Chyi, Appl. Phys. Lett. **82**, 4268 (2003).
[38]Y. Wang, X. Pei, Z. Xing, L. Guo, H. Jia, H. Chen, and J. Zhou, Jpn. J. Appl. Phys., Part 1 **46**, 4079 (2007).
[39]B. Monemar, P. Paskov, G. Pozina, J. Bergman, S. Kamiyama, M. Iwaya, H. Amano, and I. Akasaki, Phys. Status Solidi A **192**, 21 (2002).
[40]P. Lefebvre, A. Morel, M. Gallart, T. Taliercio, J. Allegre, B. Gil, H. Mathieu, B. Damilano, N. Grandjean, and J. Massies, Appl. Phys. Lett. **78**, 1252 (2001).
[41]T. J. Badcock, P. Dawson, M. J. Davies, M. J. Kappers, F. C.-P. Massabuau, F. Oehler, R. A. Oliver, and C. J. Humphreys, J. Appl. Phys. **115**, 113505 (2014).
[42]C.-N. Brosseau, M. Perrin, C. Silva, and R. Leonelli, Phys. Rev. B **82**, 085305 (2010).
[43]Y. Narukawa, Y. Kawakami, S. Fujita, S. Fujita, and S. Nakamura, Phys. Rev. B **55**, R1938 (1997).
[44]J. A. Davidson, P. Dawson, T. Wang, T. Sugahara, J. W. Orton, and S. Sakai, Semicond. Sci. Technol. **15**, 497 (2000).
[45]P. G. Eliseev, P. Perlin, J. Lee, and M. Osinski, Appl. Phys. Lett. **71**, 569 (1997).
[46]O. Rubel, M. Galluppi, S. D. Baranovskii, K. Volz, L. Geelhaar, H. Riechert, P. Thomas, and W. Stolz, J. Appl. Phys. **98**, 063518 (2005).
[47]O. Rubel, S. D. Baranovskii, K. Hantke, B. Kunert, W. W. Rühle, P. Thomas, K. Volz, and W. Stolz, Phys. Rev. B **73**, 233201 (2006).
[48]S. Hammersley, D. Watson-Parris, P. Dawson, M. J. Godfrey, T. J. Badcock, M. J. Kappers, C. McAleese, R. A. Oliver, and C. J. Humphreys, J. Appl. Phys. **111**, 083512 (2012).
[49]Y.-H. Cho, G. H. Gainer, A. J. Fischer, J. J. Song, S. Keller, U. K. Mishra, and S. P. DenBaars, Appl. Phys. Lett. **73**, 1370 (1998).
[50]M. Gurioli, A. Vinattieri, J. Martinez-Pastor, and M. Colocci, Phys. Rev. B **50**, 11817 (1994).
[51]P. G. Eliseev, J. Appl. Phys. **93**, 5404 (2003).
[52]Q. Li, S. J. Xu, M. H. Xie, and S. Y. Tong, J. Phys.: Condens. Matter **17**, 4853 (2005).
[53]C.-K. Sun, T.-L. Chiu, S. Keller, G. Wang, M. S. Minsky, S. P. DenBaars, and J. E. Bowers, Appl. Phys. Lett. **71**, 425 (1997).
[54]B. Monemar, J. Bergman, J. Dalfors, G. Pozina, B. Sernelius, P. Holtz, H. Amano, and I. Akasaki, MRS Proc. **537**, G2.5 (1998).
[55]M. Gladysiewicz, R. Kudrawiec, M. Syperek, J. Misiewicz, M. Siekacz, G. Cywinski, A. Khachapuridze, T. Suski, and C. Skierbiszewski, Appl. Phys. A **115**, 1015 (2014).
[56]T. Langer, H.-G. Pietscher, F. A. Ketzer, H. Jönen, H. Bremers, U. Rossow, D. Menzel, and A. Hangleiter, Phys. Rev. B **90**, 205302 (2014).
[57]H.-C. Wang, S.-C. Lin, Y.-C. Lu, Y.-C. Cheng, C. C. Yang, and K.-J. Ma, Appl. Phys. Lett. **85**, 1371 (2004).